

PAPER

# Quantum many-body simulation using monolayer exciton-polaritons in coupled-cavities

To cite this article: Hai-Xiao Wang *et al* 2017 *J. Phys.: Condens. Matter* **29** 445703

View the [article online](#) for updates and enhancements.

## Related content

- [Supplementary data](#)
- [Quantum simulations and many-body physics with light](#)  
Changsuk Noh and Dimitris G Angelakis
- [Quantum simulation with interacting photons](#)  
Michael J Hartmann

# Quantum many-body simulation using monolayer exciton-polaritons in coupled-cavities

Hai-Xiao Wang<sup>1</sup>, Alan Zhan<sup>2</sup>, Ya-Dong Xu<sup>1</sup>, Huan-Yang Chen<sup>2</sup>,  
Wen-Long You<sup>1</sup>, Arka Majumdar<sup>2,4</sup> and Jian-Hua Jiang<sup>1</sup> 

<sup>1</sup> College of Physics, Optoelectronics and Energy, Collaborative Innovation Center of Suzhou Nano Science and Technology, Soochow University, 1 Shizi Street, Suzhou 215006, People's Republic of China

<sup>2</sup> Department of Physics, University of Washington, Seattle, WA 98195, United States of America

<sup>3</sup> Institute of Electromagnetics and Acoustics and Department of Electronic Science, Xiamen University, Xiamen 361005, People's Republic of China

<sup>4</sup> Department of Electrical Engineering, University of Washington, Seattle, WA 98195, United States of America

E-mail: [wlyou@suda.edu.cn](mailto:wlyou@suda.edu.cn), [arka@uw.edu](mailto:arka@uw.edu) and [jianhuajiang@suda.edu.cn](mailto:jianhuajiang@suda.edu.cn)

Received 9 June 2017, revised 16 August 2017

Accepted for publication 30 August 2017

Published 12 October 2017



CrossMark

## Abstract

Quantum simulation is a promising approach to understanding complex strongly correlated many-body systems using relatively simple and tractable systems. Photon-based quantum simulators have great advantages due to the possibility of direct measurements of multi-particle correlations and ease of simulating non-equilibrium physics. However, interparticle interaction in existing photonic systems is often too weak, limiting the potential for quantum simulation. Here we propose an approach to enhance the interparticle interaction using exciton-polaritons in MoS<sub>2</sub> monolayer quantum dots embedded in 2D photonic crystal microcavities. Realistic calculation yields optimal repulsive interaction in the range of 1–10 meV—more than an order of magnitude greater than the state-of-the-art value. Such strong repulsive interaction is found to emerge neither in the photon-blockade regime for small quantum dot nor in the polariton-blockade regime for large quantum dot, but in the crossover between the two regimes with a moderate quantum-dot radius around 20 nm. The optimal repulsive interaction is found to be largest in MoS<sub>2</sub> among commonly used optoelectronic materials. Quantum simulation of strongly correlated many-body systems in a finite chain of coupled cavities and its experimental signature are studied via the exact diagonalization of the many-body Hamiltonian. A method to simulate 1D superlattices for interacting exciton-polariton gases in serially coupled cavities is also proposed. Realistic considerations on experimental realizations reveal advantages of transition metal dichalcogenide monolayer quantum dots over conventional semiconductor quantum emitters.

Keywords: exciton-polariton, monolayer materials, quantum simulation

(Some figures may appear in colour only in the online journal)

## 1. Introduction

Solving strongly correlated quantum many-body systems exactly is a formidable task. One promising approach is to mimic such complicated systems using another simpler and easily controllable quantum system, as envisioned by Feynman

[1]. To that end, the first demonstration of quantum phase transition with ultracold atoms in an optical lattice sparked a large body of research on quantum simulation in ultracold atomic systems [2, 3]. Interacting photons also provide a unique and distinctive platform to study strongly correlated quantum many-body systems [4–8]. The main idea behind this approach is to

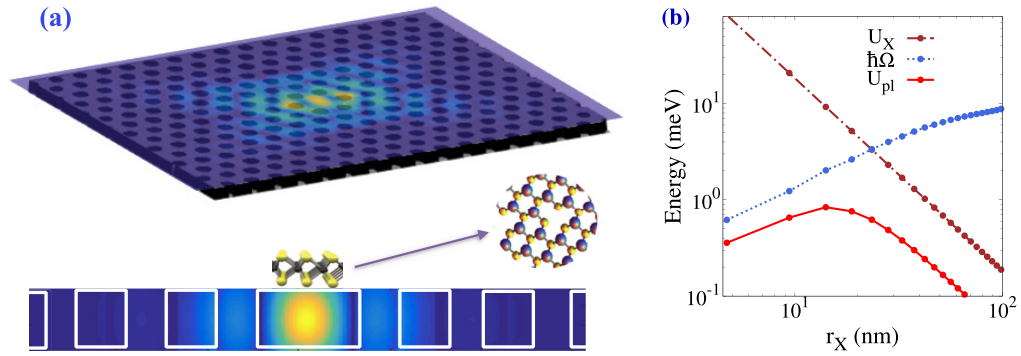


**Figure 1.** (a) Cavity-QD hybrid system for strongly interacting polaritons. Upper panel: The H1 cavity will be realized using a thin 2D photonic crystal slab. A MoS<sub>2</sub> QD is placed at the center of the cavity. Lower panel: In-plane electric field distribution in the  $x$ - $z$  plane (field outside the membrane is not plotted). The position of the MoS<sub>2</sub> QD is illustrated using a schematic of atomic structure of MoS<sub>2</sub>. (b) Exciton–exciton interaction  $U_X$ , exciton–photon interaction  $\hbar\Omega$ , and polariton–polariton interaction  $U_{pl}$  as functions of the QD radius  $r_X$  for MoS<sub>2</sub> with zero detuning.

create an interacting ‘quantum fluid of light’ [9] via a coupled network of nonlinear photonic cavities [4–11]. Advantages of photonic quantum simulators include much higher energy scale and faster operations, available non-destructive techniques for direct measurements of quasiparticle properties via spatial- and/or time-resolved multi-photon correlation functions, and abundant optical methods for coherent control [9, 12]. Such multi-particle correlation measurement is extremely difficult in both cold-atomic gases and strongly correlated electronic materials. These advantages yield great promises for photonic quantum many-body simulation as a way to understand the role of many-body quantum entanglement in Mott insulators which remains an outstanding challenge to fundamental physics [13].

Polariton, a quantum superposition of a photon and an exciton, emerges in hybrid strongly coupled systems of photonic microcavity and semiconductor excitons [11, 14]. The composite nature of polaritons leads to various unusual properties, such as high-temperature Bose–Einstein condensation (BEC) [14–17], and enhanced optical nonlinearity for applications in all-optical diodes [18] and transistors [19]. However, optical nonlinearity in those systems generally requires high polariton densities. Achieving optical nonlinearity at the single photon level requires significant reduction of the cavity mode-area/volume and optimization of the optoelectronic material (typically forming a semiconductor quantum dot (QD)) [20]. Note that, such single photon nonlinearity is necessary to realize the aforementioned photonic quantum simulators. Photon blockade, the effect where a single photon repels other photons, has been observed using a very small QD coupled to a cavity [21–24]. In those systems, Pauli blockade forbids double-occupancy of excitons, hence the interaction between polaritons is simply given by the energy difference between free polaritons and the Pauli blockade polaritons, i.e.  $U_{pl} = (2 - \sqrt{2})\hbar\Omega$ , where  $\hbar\Omega$  denotes the exciton–photon interaction strength [21–23]. However, the area of QD  $\sim (10 \text{ nm})^2$ , is much smaller than the modal area of the optical cavity, leading to much reduced light-matter interaction and polariton–polariton repulsion. The state-of-the-art value of polariton repulsive interaction in the photon-blockade regime is less than 0.1 meV [24]. Thus an important challenge for polariton quantum many-body simulation is to realize much stronger repulsive interaction.

In this work, we propose an optoelectronic architecture to realize polariton repulsion much larger than the state-of-the-art value,  $1 \sim 10$  meV, using exciton–polaritons based on monolayer MoS<sub>2</sub> QDs embedded in slab photonic crystal cavities. The strength of the repulsive interaction varies with the quantum dot radius due to the competition between the exciton–photon interaction and the exciton–exciton repulsion. It is found that the strongest repulsive interaction emerges neither in the photon-blockade regime for small QDs nor in the polariton-blockade regime for large QDs, but in the crossover between the two regimes. An optimal quantum dot radius is found as  $\sim 20$  nm. Similar trends are found for other common materials such as GaAs, InAs, CdTe, and GaN. Nevertheless, MoS<sub>2</sub> provides the largest nonlinearity, thanks to strong light-matter and exciton–exciton interactions. We further investigate possible experimental consequences of quantum simulation in a chain of coupled cavities using exact diagonalization of the many-body Hamiltonian. In addition, a method for simulation of superlattices in coupled cavities is proposed and the regimes for Mott transition is estimated using single- and two-particle analysis. Realistic considerations for fabrication and measurements reveal advantages of transition metal dichalcogenide (TMD) monolayer semiconductors over conventional optoelectronic materials.

## 2. Material and photonic architecture

The proposed architecture is illustrated in figure 1(a). The cavity is formed by a point defect in a 2D hexagonal photonic crystal slab, also known as the H1 cavity [25] (see appendix A). The fundamental mode of the H1 cavity is non-degenerate. Because of this fact and the time-reversal symmetry, the cavity photon is a 50%–50% mixture of the left- and right- circular polarizations. Thus the cavity photon couples equally with the two valleys of MoS<sub>2</sub>. In the quasi-equilibrium states of the exciton-polariton, the valley coherence is maintained during the exciton-polariton lifetime. Since the cavity suppresses the exciton radiative decay, the exciton-polaritons are expected to have longer lifetimes. Exciton-polariton decay in this regime is mainly caused by the nonradiative recombination of exciton [51], which takes more than 70 ps in MoS<sub>2</sub>. The MoS<sub>2</sub> QDs

can be fabricated by patterning a MoS<sub>2</sub> monolayer and placing the patterned film on top of the slab photonic crystal cavity. A network of the cavity-QD hybrid structure forms an interacting polariton lattice system, which is described by the following Hamiltonian [9]

$$\mathcal{H} = \sum_i [\hbar\omega_c c_i^\dagger c_i + \hbar\omega_X b_i^\dagger b_i + \hbar\Omega(c_i b_i^\dagger + b_i c_i^\dagger) + \frac{1}{2} U_X \mathcal{N}_i (\mathcal{N}_i - 1)] - t \sum_{\langle i,j \rangle} c_i^\dagger c_j. \quad (1)$$

Here  $\omega_c$  is the frequency of the cavity mode,  $c_i^\dagger$  ( $b_i^\dagger$ ) creates a photon (exciton) in the  $i^{\text{th}}$  cavity (QD),  $\mathcal{N}_i = b_i^\dagger b_i$  stands for the exciton number operator,  $U_X$  denotes the exciton–exciton repulsion,  $\hbar\Omega$  represents the exciton–photon interaction, and  $\hbar\omega_X = 1.87$  eV is the exciton energy in MoS<sub>2</sub> QDs. We assume that  $\omega_c$  is identical for each cavity and  $\omega_X$  is the same for each MoS<sub>2</sub> QD. The effects of fluctuation and disorder will be considered later. From [14, 17], the exciton–photon coupling is

$$\hbar\Omega = \frac{d_{\text{cv}} |\phi(0)| \sqrt{\hbar\omega_c}}{\sqrt{2\epsilon_0 L_c}}, \quad (2)$$

where  $d_{\text{cv}} = 4.0 \times 10^{-29}$  C · m is the interband dipole matrix element [17, 26] and  $|\phi(0)| = \sqrt{2/(\pi a_B^2)}$  is the exciton wave amplitude at zero electron-hole distance ( $a_B = 1$  nm is the exciton Bohr radius in MoS<sub>2</sub> [27]). The exciton–photon coupling depends on the following quantity of the dimension of length,

$$L_c \equiv \frac{\int_c d\vec{r} \epsilon(\vec{r}) |\vec{E}(\vec{r})|^2}{\int_c dx dy |\vec{E}(x, y, z_0)|^2 \Theta(x, y, z_0)}, \quad (3)$$

where  $\epsilon(\vec{r})$  is the position-dependent (relative) dielectric constant,  $\vec{E}(\vec{r})$  is the electric field of the cavity mode, and  $z_0$  is the  $z$  coordinate of the MoS<sub>2</sub> monolayer. The  $\Theta(x, y, z_0)$  function, which takes into account the finite overlap between the QD and the cavity optical field, is unity in the QD region and zero outside [14]. The integrals are carried out within each cavity. The exciton–exciton interaction strength is given by [28]  $U_X = \frac{6E_b a_B^2}{S_X}$ , where  $E_b = 0.96$  eV is the exciton binding energy and  $S_X = \pi r_X^2$  is the area of the circular MoS<sub>2</sub> QD with radius  $r_X$ . The last term in equation (1) describes photon hopping between nearest-neighbor cavities, where  $t$  is the hopping energy. Note that in the above formalism, the exciton-polariton is approximately treated as uniformly distributed in the QDs (resulting in  $\Theta(x)$  in equation (3) and the  $S_X$  factor in  $U_X$ ). More rigorous treatment with non-uniform distribution is equivalent to a correction of the effective area of the polariton, which affects the results marginally (see appendix B).

The designed H1 cavity has a slab thickness of 110 nm and a lattice periodicity of  $a = 190$  nm to ensure that the fundamental TE mode is resonant with the MoS<sub>2</sub> exciton ( $\lambda_X = 660$  nm;  $\lambda_X$  is the photon wavelength in vacuum for frequency  $\omega_X$ ). Gallium phosphide is chosen as the material for the slab photonic crystal cavity, due to its high refractive index ( $n = 3.2$ ) and transparency in that wavelength range. The choice of H1 cavity is primarily motivated by its small mode-volume ( $\sim 0.45(\lambda_X/n)^3$ ) and mode area ( $\sim (\lambda_X/n)^2$ ).

### 3. Effective Hamiltonian and polariton–polariton interaction

In the uncoupled limit, photon is itinerant and exciton is localized. All interesting physics comes in when the light-matter interaction is turned on. In the regime when the light-matter interaction  $\hbar\Omega$  is much greater than the photon hopping  $t$  [7], the many-body quantum dynamics close to the ground state is constrained to the lower-polariton Hilbert space and one can truncate the full Hamiltonian (1) into the following effective Hamiltonian [9]

$$\mathcal{H}_{\text{pl}} = -t_{\text{pl}} \sum_{\langle i,j \rangle} a_i^\dagger a_j + \frac{1}{2} \sum_i U_{\text{pl}} n_i (n_i - 1). \quad (4)$$

Here  $t_{\text{pl}} = t p_c$  and  $n_i = a_i^\dagger a_i$  with  $a_i^\dagger$  being polariton creation operator.  $p_c \equiv \cos^2[\frac{1}{2} \text{arccot}(\frac{\Delta}{2\hbar\Omega})]$  is the photonic fraction of the lower polariton [9], where  $\Delta \equiv \hbar(\omega_X - \omega_c)$  is the exciton–photon detuning. The polariton–polariton interaction  $U_{\text{pl}}$  is determined by the difference between the ground state energy of an isolated cavity with two quanta with and without the exciton–exciton repulsion, respectively [7],

$$U_{\text{pl}} \equiv E_{\text{GS}}(2q) - E_{\text{GS}}^{(0)}(2q). \quad (5)$$

The ground state energy of the polaritonic system is calculated based on the following: The Hamiltonian of an isolated cavity with two energy quanta can be written in the basis of  $(|2, 0\rangle, |1, 1\rangle, |0, 2\rangle)^T$  (here  $|n_p, n_x\rangle$  with  $n_p + n_x = 2$  are the Fock states with  $n_p$  photons and  $n_x$  excitons) as

$$\mathcal{H}_{2q} = \begin{pmatrix} 2\hbar\omega_c & \sqrt{2}\hbar\Omega & 0 \\ \sqrt{2}\hbar\Omega & \hbar(\omega_c + \omega_X) & \sqrt{2}\hbar\Omega \\ 0 & \sqrt{2}\hbar\Omega & 2\hbar\omega_X + U_X \end{pmatrix}. \quad (6)$$

The ground state of the above Hamiltonian consists of two interacting polaritons, of which the total energy is  $E_{\text{GS}}(2q)$ . When the interaction between exciton is turned off,  $U_X = 0$ , the ground state of the Hamiltonian gives two noninteracting polaritons, with total energy  $E_{\text{GS}}^{(0)}(2q)$ . The difference between the two energies of the ground states is the interaction energy between two polaritons within a cavity.

In the literature, there are two distinct regimes in which photon antibunching were observed and studied: (i) the photon blockade regime [21–24] where the QD size is small and thus  $U_X \gg \hbar\Omega$ , (ii) the polariton blockade regime [20] where the QD size is large and then  $U_X \ll \hbar\Omega$ . Photon blockade was observed experimentally in cavity-QD hybrid systems using small InAs QDs where the value of exciton–photon coupling strength is small,  $\hbar\Omega \leq 0.16$  meV [24]. In these systems the polariton interaction  $U_{\text{pl}}$  is weak,  $U_{\text{pl}} \leq 0.1$  meV [24].

One of the main conclusions in this paper is that the maximum polariton–polariton interaction is not reached in the photon blockade regime where the exciton–exciton repulsion is very strong, nor in the polariton blockade regime where the light-matter interaction is very strong. As illustrated in figure 1(b), the polariton–polariton interaction  $U_{\text{pl}}$  ramps up when the QD radius  $r_X$  is small (the photon blockade regime). After reaching to a maximum value around  $r_X = 20$  nm,  $U_{\text{pl}}$

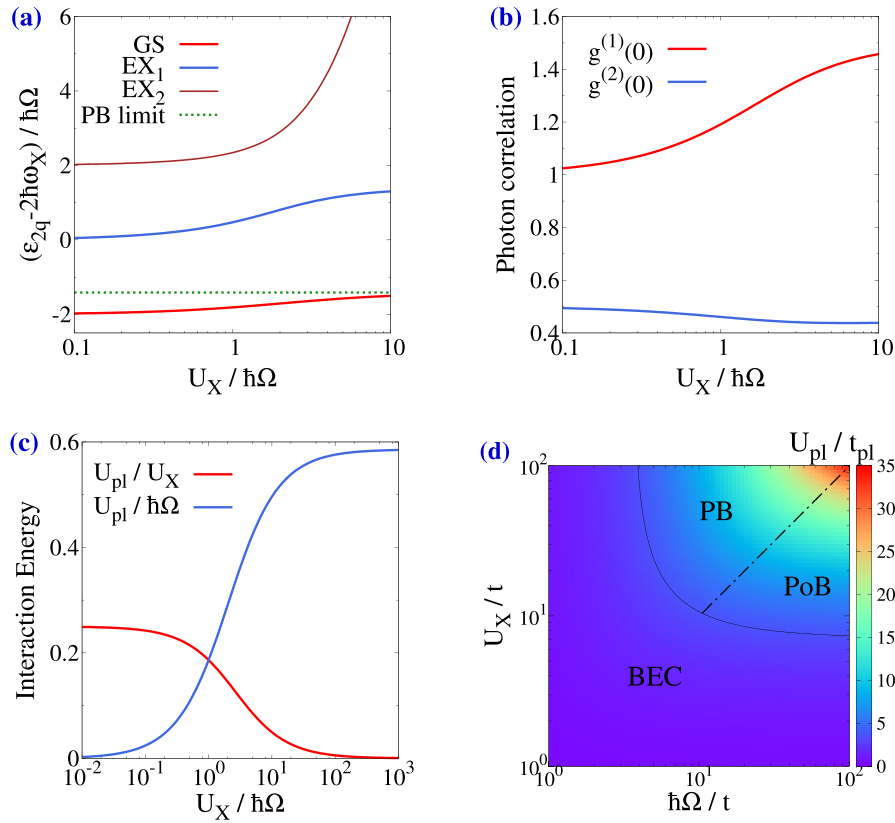


**Figure 2.** Crossover from polariton blockade to photon blockade. (a) Energy levels  $\epsilon_{2q}$  of the ground state (GS), the first and second excited states ( $EX_1$  and  $EX_2$ ) as functions of the exciton–exciton interaction  $U_X$  for a single cavity with two energy quanta. We scale the interaction energy  $U_X$  with the exciton–photon coupling  $\hbar\Omega$ . The dotted line denote the energy  $-\sqrt{2}\hbar\Omega$ , i.e. the GS energy in the photon blockade (PB) limit. (b) Photon correlation function  $g^{(1)}(0)$  and  $g^{(2)}(0)$  as functions of  $U_X/(\hbar\Omega)$ . (c) Polariton interaction energy  $U_{pl}$  for various  $U_X/(\hbar\Omega)$ . (d)  $\alpha$  and phase diagram of 1D interacting polaritons with zero detuning. The Mott insulator phase consists of two regions: the PB region and the polariton blockade (PoB) region. The phase boundary between BEC and Mott insulator is labeled by the solid curve, while the crossover between PB and PoB regions is labeled by the chained curve.

decays with the QD radius in the polariton blockade regime. The maximum value of  $U_{pl}$  lies in the crossover between the two regimes. To the best of our knowledge such non-monotonic behavior (also holds for other materials, see appendix C) is never reported before. This finding indicates that there is an optimal QD radius for strong polariton–polariton interaction in each optoelectronic material.

To understand the underlying physics, we calculate the spectrum and photon correlation of the isolated cavity with two energy quanta. The energy levels of the Hamiltonian equation (6), denoted as  $\epsilon_{2q}$ , as functions of the repulsive interaction  $U_X$  are given in figure 2(a). The photon blockade limit (i.e. when exciton repulsion  $U_X$  is much larger than the exciton–photon coupling  $\hbar\Omega$ ) is represented by the dotted line. We find that the ground state energy  $E_{GS}(2q)$  indeed increases with exciton–exciton repulsion  $U_X$  (see figure 2(a)) and the photon antibunching is stronger in the strong exciton repulsion regime (see figure 2(b)). In this regime the first-order correlation function becomes greater than unity, as the manifestation of the projection out of the double exciton state (i.e. the 2nd excited state in figure 2(a)) due to strong exciton repulsion.

However, as shown in figure 1(b), strong exciton–exciton repulsion requires very small QD radius. Unfortunately for such small QD the light-matter interaction  $\hbar\Omega$  is very small (due to much reduced overlap between the exciton and the

**Table 1.** Properties of exciton-polaritons for MoS<sub>2</sub>, MoSe<sub>2</sub>, GaAs, CdTe, InAs, and GaN QDs in H1 cavity at zero exciton–photon detuning.

Material	Optimal $U_{pl}$ (meV)	$g_X$ (meV)	$\lambda_X$ (nm)	$U_X^0$ (meV)
MoS <sub>2</sub>	0.85	36.	660	0.013
MoSe <sub>2</sub>	0.48	20.	790	0.0076
GaAs	0.32	11.	700	0.0082
CdTe	0.33	20.	750	0.0030
InAs	0.16	7.1	1310	0.0024
GaN	0.51	17.	340	0.014

photon field) and the polariton–polariton repulsive interaction is determined by  $U_{pl} \simeq (2 - \sqrt{2})\hbar\Omega$  (see figure 2(c)). Thus the polariton interaction  $U_{pl}$  is rather weakened with decreasing QD size in this regime, as indicated in figure 1(b).

In the other limit, when the light-matter interaction  $\hbar\Omega$  is much stronger than the exciton–exciton repulsion  $U_X$ , the polariton interaction  $U_{pl}$  is limited by the exciton–exciton repulsion  $U_X$  (see figure 2(c)). In this regime, increasing the QD size leads to greater light-matter interaction  $\hbar\Omega$  but reduced exciton repulsion  $U_X$  (since  $U_X = 6E_b a_B^2 / S_X$ ). Therefore, the polariton interaction  $U_{pl}$  decreases with increasing QD size. Following these reasonings, the non-monotonic dependence

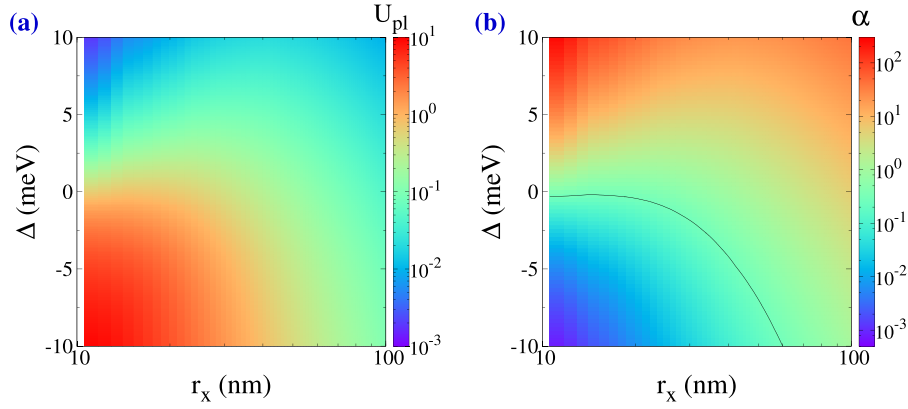


**Figure 3.** (a) Polariton–polariton interaction  $U_{\text{pl}}$  versus  $r_X$  and exciton–photon detuning  $\Delta$ . (b)  $\alpha$  and phase diagram for strongly interacting 1D polariton system for various MoS<sub>2</sub> QD radius  $r_X$  and exciton–photon detuning  $\Delta$  with hopping energy  $t = 0.5$  meV.

of the polariton–polariton interaction  $U_{\text{pl}}$  on the QD size shown in figure 1(b) is an universal behavior for all quantum-emitters. Indeed, we find that this behavior holds true for other common quantum emitters, such as GaAs, InAs, CdTe, GaN and MoSe<sub>2</sub> QDs. The optimal polariton–polariton interaction for all these quantum-emitters are listed in table 1. The calculation details and material parameters are presented in appendix C. We find that MoS<sub>2</sub> is one of the best material for strong polariton–polariton repulsion. The other TMD material, MoSe<sub>2</sub>, is also very appealing for strong polariton repulsion. We define and calculate the following quantities to measure the typical exciton–photon coupling, photon wavelength, and exciton–exciton interaction strength,

$$g_X \equiv \frac{d_{\text{cv}}|\phi(0)|\sqrt{\hbar\omega_X}}{\sqrt{2\epsilon_0\lambda_X}}, \quad \lambda_X \equiv \frac{2\pi c}{\omega_X}, \quad U_X^0 \equiv \frac{6E_b a_B^2}{\lambda_X^2}. \quad (7)$$

Their values are also listed in table 1. We find that the exciton–photon and exciton–exciton interactions are both very strong in MoS<sub>2</sub>, which leads to strong polariton repulsion  $U_{\text{pl}}$ . The most promising IIIV semiconductor is GaN, which however has a very small photon wavelength  $\lambda_X$ . Therefore, it requires much smaller holes and lattice constant for the slab photonic crystal cavity, which is challenging to fabricate within current technology. Finally, we remark that if light-trapping in the cavity can be enhanced, i.e. the ratio of the mode area to  $\lambda_X^2$  can be decreased, the polariton repulsion can be further increased.

We now illustrate the phase diagram of the 1D interacting polariton system at zero exciton–photon detuning in figure 2(d). The polariton Mott insulator phase exists in the region with *simultaneous* strong exciton–exciton interaction and strong exciton–photon interaction. The whole region can be separated into two regimes: the polariton-blockade regime and the photon-blockade regime. The crossover line (the dot-dashed line) is determined by  $U_X = \hbar\Omega$ . In the other regions the polariton–polariton interaction  $U_{\text{pl}}$  is not strong enough to drive the Mott transition, hence the system is in the BEC phase of polaritons. The Mott-BEC phase boundary is evaluated approximately via  $\alpha = \alpha_c$  ( $\alpha \equiv t_{\text{pl}}/U_{\text{pl}}$ ) with  $\alpha_c = 0.28$  for filling factor  $\nu = 1$  (i.e. one polariton per cavity) [29].

Using the material parameters of MoS<sub>2</sub> QD, we calculate the polariton–polariton interaction  $U_{\text{pl}}$  and the dimensionless parameter  $\alpha$  for various detuning  $\Delta$  and QD radius  $r_X$  (see figures 3(a)

and (b)). The polariton–polariton interaction can be greater than 1 meV for MoS<sub>2</sub> for negative detuning. However, at too large negative detuning, the polaritons behave like an exciton, and impedes photonic quantum simulation as the photon addressability of the polaritons is significantly reduced. From figure 3(a) the accessible polariton repulsion can be as large as several meV. The dimensionless parameter  $\alpha$  gives the parameter regimes for polariton Mott insulator, where the phase boundary is evaluated again via  $\alpha = \alpha_c$  as indicated by the black curve.

To confirm the above findings, we performed full quantum optical simulation of a tuned single H1-cavity—MoS<sub>2</sub>-QD hybrid structure, in presence of the excitonic and photonic losses. In our simulations, the excitonic loss rate  $\gamma_X$  and photonic loss rate  $\gamma_c$  are assumed to be same ( $\gamma_X = \gamma_c = 2\pi$  GHz). We numerically calculate the evolution of the density matrix by using the standard Lindblad formalism [30, 31]. The calculated second-order correlation function  $g^{(2)}(0)$  shows that the photon-antibunching takes place at the lower-polariton frequency  $\omega = \omega_X - \Omega$ , corresponding to a dip in the auto-correlation function  $g^{(2)}(0)$  (see figures 4(a) and (b)). This is consistent with both the pictures of photon blockade and polariton blockade. On the high-frequency shoulder close to the dip, there always exists a peak of the second-order correlation  $g^{(2)}(0)$  (see figures 4(a) and (c)). This photon bunching corresponds to the resonant excitation of double occupancy of interacting polaritons (i.e. adding another polariton to a cavity that already has one polariton). Therefore, the frequency difference between the peak and the dip,  $\omega_{\text{peak}} - \omega_{\text{dip}} = \omega_{\text{peak}} - \omega_X + \Omega \simeq U_{\text{pl}}/\hbar$ , gives a good evaluation of the polariton interaction strength  $U_{\text{pl}}$ . This frequency difference is indeed maximized for the QD radius slightly below 20 nm (see figure 4(d)). Both the photon antibunching at the dip and the bunching at the peak become very significant for that optimized QD radius (see figures 4(b) and (c)).

#### 4. Quantum many-body simulation in a finite chain of coupled cavities

The effect of strong interaction between polaritons can be characterized by the second- and third- order correlation functions which can be measured experimentally [12]. We have

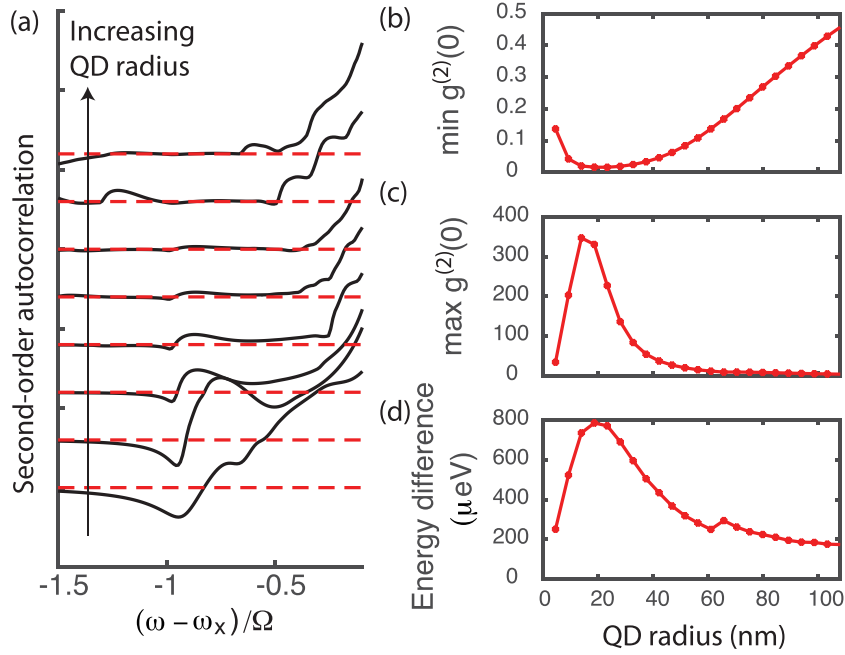


**Figure 4.** (a) Second-order autocorrelation  $g^{(2)}(0)$  versus optical frequency  $\omega$  for various QD radius for a MoS<sub>2</sub> QD in a single cavity as calculated using the Lindblad formalism. The correlation function  $g^{(2)}(0)$  has a dip (antibunching) at the lower-polariton frequency,  $\omega_x - \Omega$ , and a peak (bunching) on the high-frequency shoulder close to the dip. (b) The minimum  $g^{(2)}(0)$  at the dip, (c) the maximum  $g^{(2)}(0)$  on the high-frequency shoulder versus the QD radius as extracted from (a). (d) The frequency difference (as converted to energy difference) between the dip and the peak versus the QD radius. The detuning of the quantum emitter and the photon cavity is  $\Delta = 0$ .

studied such correlation functions for single cavities in the previous sections. We now show that these correlations can also extract useful information of the complex many-body ground state wavefunction of a finite 1D chain of serially coupled cavities.

We calculate the ground state wavefunction of a 1D lattice of interacting polaritons using exact diagonalization method. We use periodic boundary condition for  $N = 10$  sites where each site can have a maximum of three polaritons. We note that for a chain of cavities, we did not consider loss, as a full master equation simulation of the whole chain is computationally intractable due to extremely large Hilbert space. While this is a limitation of the present theoretical treatment, it is the same reason why quantum simulation is highly sought after. The ground state wavefunction of the system is very complex. It contains many kinds of long-range multi-particle entanglement [13]. A way to characterize such entanglement is to measure the multi-photon correlations. We calculate the following correlation functions using the many-body *ground state* obtained from exact diagonalization of the Bose-Hubbard Hamiltonian (4):

$$g_{ij}^{(2)}(0) = \frac{\langle a_i^\dagger a_j^\dagger a_i a_j \rangle}{\langle a_i^\dagger a_i \rangle \langle a_j^\dagger a_j \rangle}, \quad (8)$$

$$g_{i \neq j \neq l}^{(3)}(0) = \frac{\langle n_i n_j n_l \rangle}{\langle n_i \rangle \langle n_j \rangle \langle n_l \rangle}, \quad (9)$$

where  $n_i = a_i^\dagger a_i$ . In the regime where  $\hbar\Omega \gg t$  the lower polariton picture is well-defined, the  $g_{ij}^{(2)}(0)$  correlation function is proportional to the second-order photon correlation

that can be determined via Hanbury Brown and Twiss measurements. We calculate  $g^{(2)}(0)$  and  $g^{(3)}(0)$  for the ground state with various  $U_{\text{pl}}/t_{\text{pl}}$  (results are shown in figures 5(a) and (b)). The second-order correlation function at the same site  $g_{ii}^{(2)}(0)$  decreases quickly with increasing  $U_{\text{pl}}/t_{\text{pl}}$ , which signifies photon antibunching due to strong polariton repulsion. On the other hand  $g^{(2)}(0)$  at different sites increases with increasing  $U_{\text{pl}}/t_{\text{pl}}$ , consistent with the understanding that the Mott insulator state is mostly a product state (plus quantum fluctuations) with each site occupied by a single polariton. Figure 5(b) shows the build-up of  $g^{(3)}(0)$  correlations with increasing  $U_{\text{pl}}/t_{\text{pl}}$  which signifies the localization of polaritons due to their mutual repulsion. Those correlation functions reveal the complex inter-particle entanglement in the strongly interacting polariton systems which can be sources for non-classical, highly-entangled light.

We also computed the following structure factors

$$S_1(k) = \frac{1}{N} \sum_j \langle a_i^\dagger a_j \rangle e^{ik(i-j)/N}, \quad (10)$$

$$S_2(k) = \frac{1}{N} \sum_j \langle n_i n_j \rangle e^{ik(i-j)/N}, \quad (11)$$

as well as the visibility fringes [5–7]

$$\mathcal{V}_1 = \frac{S_1|_{\max} - S_1|_{\min}}{S_1|_{\max} + S_1|_{\min}}, \quad (12)$$

$$\mathcal{V}_2 = \frac{S_2|_{\max} - S_2|_{\min}}{S_2|_{\max} + S_2|_{\min}}. \quad (13)$$

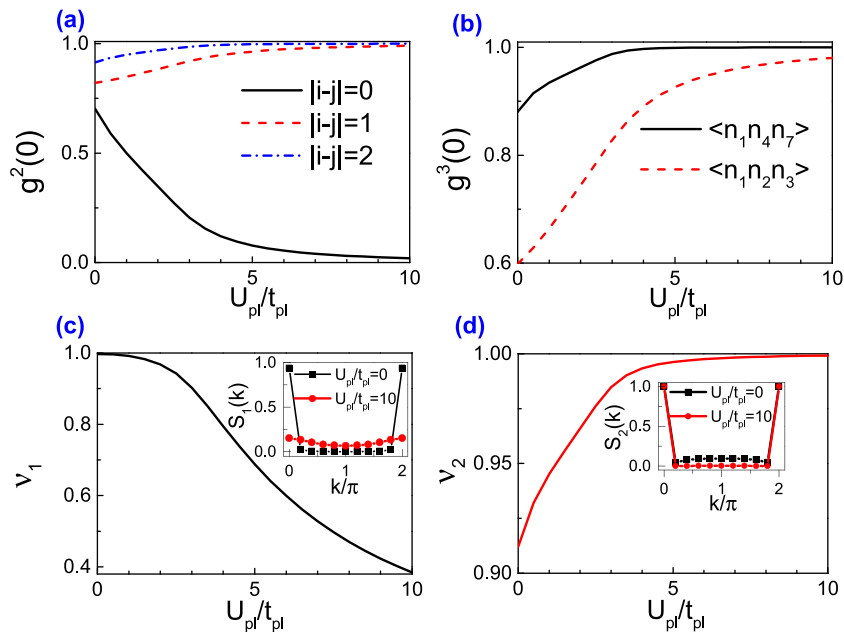


**Figure 5.** Second-order and third-order correlation function of the ground state of 1D Bose–Hubbard model equation (4). (a) Equal-time second-order correlation functions  $g^{(2)}(0)$  at the same site (black curve) and for nearby sites (red and blue curves) versus  $U_{pl}/t_{pl}$ . (b) Equal-time third-order correlations for nearby sites as functions of  $U_{pl}/t_{pl}$ . (c) The structure factor  $S_1(k)$  for photon field and visibility fringe  $\mathcal{V}_1$  for different  $U_{pl}/t_{pl}$ . (d) The structure factor  $S_2(k)$  for photon number and visibility fringe  $\mathcal{V}_2$  for various  $U_{pl}/t_{pl}$ .

The results are plotted in figures 4(c) and (d). The visibility fringe  $\mathcal{V}_1$  decreases dramatically with increasing  $U_{pl}/t_{pl}$ , which is the signature of the emergence of the Mott insulator state. On the other hand, the visibility fringe  $\mathcal{V}_2$  increases only slightly with increasing  $U_{pl}/t_{pl}$ . The visibility fringe  $\mathcal{V}_1$  has large contrast for the BEC and Mott insulator states because the BEC is a coherent state with long range single-particle correlation, while the Mott insulator is a gapped state with short-range single-particle correlation.

In the above, we discussed the phase diagram for interacting polaritons in the limit of low-temperature equilibrium phases. The preparation of these phases may encounter realistic challenges. For example, there are photonic and excitonic decays which cause dissipation and nonconservation of the quasiparticle number. This may be an issue or not, depending on the competition of time-scales of decay and other desired physical processes in the QD-cavity array (i.e. depending on the energy scales of the interaction and kinetic energy versus that of the decay rate). Also, as discussed in [5, 6], the initial state can be prepared in the Mott insulator state via pulsed excitations, the transition into the superfluid state can be observed by adiabatic tuning of the hopping between cavities which can be controlled optically. Other discussions on observing the Mott-insulator—superfluid transition through pulsed excitations are presented in [32]. If continuous pumping is used to compensate the loss, the physics becomes much richer and depends on the specific pumping scenarios and parameters [33–38]. In these works, the driven-dissipation effects are studied using Lindblad equations for many polaritons, unlike the naive exact-diagonalization method employed here which is unable to include dissipation in many-body systems. We nevertheless included the dissipation in the study of photon-bunching and antibunching

for various frequencies in a single cavity using the Lindblad equation as shown in figure 4.

## 5. Quantum simulation of superlattices of coupled cavity arrays

We now introduce a method for quantum simulation of superlattices of serially coupled cavity arrays. This can be done via modulating the detuning, for example, by making the detuning at even (odd) lattice sites as  $\Delta(-\Delta)$ . The opposite detunings at two cavities modify the single particle spectrum and the effect of interaction. The single particle spectrum of a pair of such detuned cavities is plotted in figure 6(a). The splitting between the ground state and the first excited state is  $\sqrt{\Delta^2 + t^2}$ . Thus at large detuning  $|\Delta|$  the full Hamiltonian can be truncated into the Hilbert space of the lowest energy state of a pair of cavity. In this regime each pair of cavities contribute only one single particle state (see figure 6(b)). Therefore, at half-filling  $\nu = 1/2$  the polaritons system can have phase transition into the Mott insulator state if the interaction between polaritons is strong.

We calculate the many-body ground state of a finite chain of coupled cavities (with 10 cavities) for filling factor  $\nu = 1/2$  and  $\nu = 1$  by exact diagonalization of the many-body Hamiltonian with a cut-off of the single site Hilbert space at three bosons. From the ground state wavefunction, we can obtain the second-order correlation function  $g^{(2)}(0)$  for the even sites and the odd sites. The averaged  $g^{(2)}(0)$  is more relevant to experimental measurements since it is difficult to distinguish photons from the even site or the odd site. The significant reduction of the  $g^{(2)}(0)$  correlation function below unity signifies the transition into the Mott insulator states. For

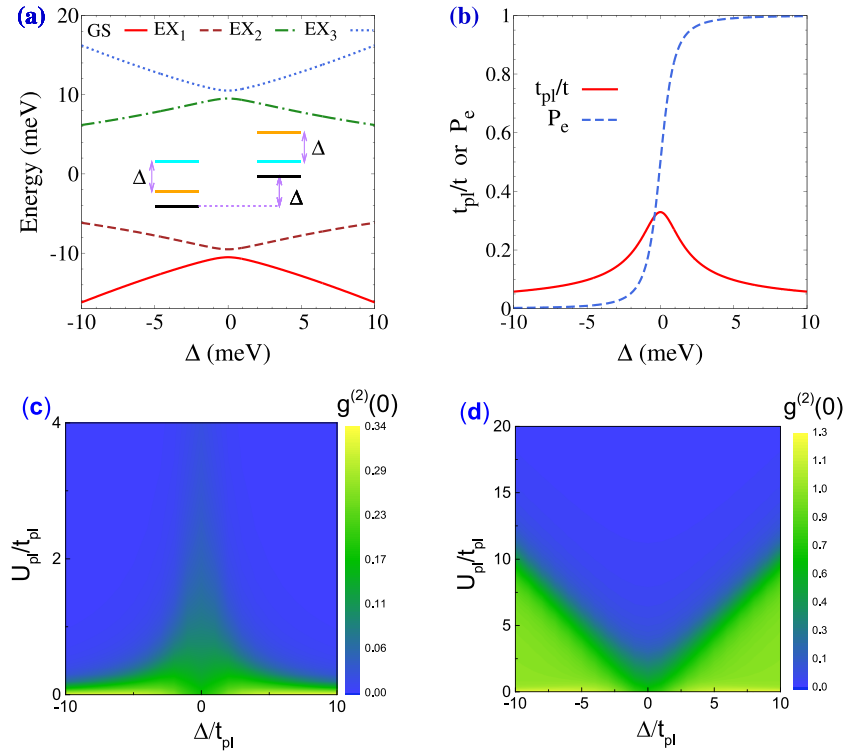


**Figure 6.** Quantum simulation in 1D Cavity-QD superlattices. (a) Single-particle energy spectrum of coupled double cavity. Inset: Left (right) is the exciton (cyan), cavity (orange), lower polariton (black) energy levels for the even (odd) sites. The detuning at the even sites is positive, while at the odd sites it is negative. The energy difference between lower polariton levels in the two different sites is just the detuning  $\Delta$ . (b) Hopping energy  $t_{pl}/t$  and the probability at even site  $P_e$  as functions of the detuning. Parameters for (a) and (b):  $t = 1$  meV and  $\hbar\Omega = 10$  meV. (c) The correlation function  $g^{(2)}(0)$  (averaged over the odd and even sites) as a function of the staggered detuning and the interaction strength for filling factor  $\nu = 1/2$  in a finite chain of ten sites. (d) Similar to (c) but with filling factor  $\nu = 1$ .

half-filling, the Mott transition is facilitated by the staggered detuning, which is consistent with the superlattice picture. For  $\nu = 1$  filling, the effective filling factor at large detuning  $|\Delta|$  is 2. Since the Mott transition at higher filling factor requires larger interaction strength, the staggered detuning impedes Mott transition in the large detuning  $|\Delta|$  regime for  $\nu = 1$ . Our numerical simulation is also inconsistent with a few-particle analysis in the appendix D.

## 6. Realistic considerations on experimental realization

It is known that lack of control over self-assembled QDs positioning thwarts the scalability of the nonlinear polariton system. Deterministic fabrication and positioning of the QDs, by patterning a quantum well like structure can potentially solve this problem. Unfortunately, such patterning of usual quantum wells degrades the exciton significantly [39]. Monolayer materials have been proven to be chemically and mechanically stable and robust [40–42], and can potentially circumvent these problems of usual optoelectronic materials.

The difficulties in precisely positioning QDs to the center of each cavity are due to incompatibility of the fabrication method of photonic crystal cavity and that of the QD. Recently new fabrication methods for MoS<sub>2</sub> monolayer QDs was developed where size and position of QDs can be controlled much more precisely than previous methods using lithography [43].

The main advantages of using MoS<sub>2</sub> monolayer QDs is its unique material compatibility, and robustness against etching (due to its mechanical and chemical stability) [44]. Recent works have demonstrated growth of a large area of monolayer material [45]. In practice one can start with such a large area of monolayer materials, and pattern it to create an array of quantum dots. The current state-of-the-art electron-beam technology can fabricate structure reliably with  $\sim 1$  nm resolution. A large uncertainty comes from the etching of the quantum well. The extent of the lateral etching in quantum well is random, which gives rise to different size of quantum dots and thus different frequency. Monolayer materials provide an excellent opportunity, because due to their extreme thinness, etching them is simple, and does not cause significant lateral etching. Hence, fabricating 20 nm radius quantum dot, and patterning them in an array with periodicity of  $\sim 200$  nm is well within the current fabrication capability. In the experiment, one can first fabricate the coupled cavity array, and then transfer the 2D material to the photonic chip. One can perform an overlay to align the monolayer quantum dots with the cavities. Note that, current electron-beam technology also provides an overlay accuracy of 1 nm. As the cavity lateral mode size is significantly bigger than 1 nm, the fluctuation in exciton–photon coupling due to QD positioning can be effectively suppressed. Since the etching processes affect the photonic crystal cavity negligibly, this method also decouples the correlation between various parameters in our model.

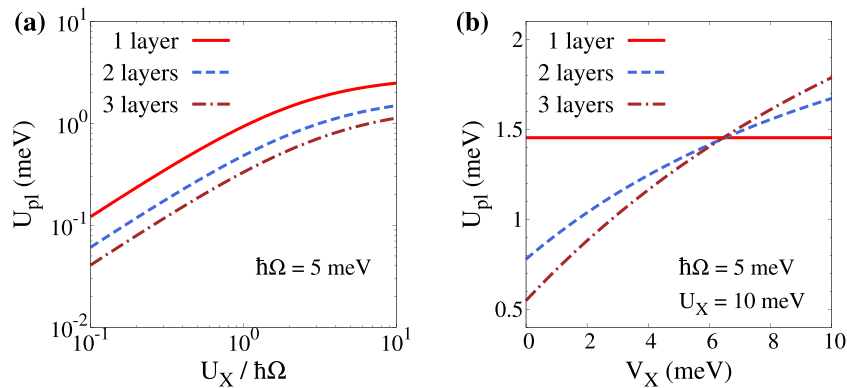


**Figure 7.** Multilayer effect. (a) Polariton repulsive interaction  $U_{pl}$  for monolayer, bilayer, and trilayer as functions of (intralayer) exciton–exciton interaction  $U_X$  in the limit of vanishing interlayer interaction  $V_X = 0$ . (b) Polariton repulsive interaction for  $U_{pl}$  for monolayer, bilayer, and trilayer as functions of interlayer exciton–exciton interaction  $V_X$  for  $U_X = 10$  meV. For both (a) and (b), the exciton–photon interaction is  $\hbar\Omega = 5$  meV.

The main dissipation mechanisms in the coupled-cavity-array system come from the finite exciton and photon lifetimes [14]. The state-of-the-art fabrication technology of photonic crystal cavity has enabled good control of cavity frequency and very high quality factors (over one million) [46]. With such fabrication technology, one can have good control of cavity resonance with wavelength uncertainty below 1 nm [46]. The finite lifetime due to exciton non-radiative decay is, however, a major challenge. Note that recent works have demonstrated good surface passivation to reduce the non-radiative recombination [47]. These experimental advancement encourages us to believe that the exciton nonradiative decay in the QDs can be as long as the exciton lifetime in the monolayer ( $\gtrsim 70$  ps). At sub-1 K temperature, exciton nonradiative decay is further suppressed, which is negligible as the resulting exciton linewidth is much smaller than other energy scales such as  $t_{pl}$  and  $U_{pl}$  ( $\sim 1$  meV).

In realistic MoS<sub>2</sub> QD-cavity systems, the MoS<sub>2</sub> QD may form not just in a monolayer but in multiple layers. The latter situation corresponds to stacking of several monolayer QD together (thus the exciton–photon interaction in these layers are the same). Most often there can be 1, 2, and 3 layers. We shall study the effect of multilayers on the polariton–polariton interaction  $U_{pl}$  within a cavity, which is calculated using equation (5). Since the nature of interlayer exciton–exciton interaction is unknown, we use a parameter  $V_X$  to characterize this interaction between excitons in adjacent QDs. Let us first consider the limit with  $V_X = 0$  as shown in figure 7(a). Our calculation gives that the polariton repulsive interaction  $U_{pl}$  decreases with increasing number of layers. This is true for both photon-blockade and polariton-blockade regimes. Physically, this is because without interlayer interaction, polaritons tend to spread over multiple layers to reduce the repulsive interaction and the ground state energy. For finite interlayer interaction  $V_X$ , the polariton repulsion in multilayer QDs increases with increasing  $V_X$ . The layer numbers become irrelevant when  $V_X \simeq 0.6U_X$ . Polariton repulsion can be enhanced in multilayer QDs for larger  $V_X$  which we believe is unlikely to be realistic, since  $V_X$  is supposed to be smaller than  $U_X$ .

## 7. Conclusion and discussions

We propose realizing strongly interacting polariton systems based on MoS<sub>2</sub> QD coupled with the H1 photonic crystal cavity. The material design enables simultaneous realization of strong exciton–photon coupling and strong exciton–exciton repulsion. This advantage results in polariton interaction one order of magnitude stronger than in the state-of-the-art single-photon quantum optical systems. The strongly interacting polariton systems can serve as a platform for quantum simulation of many-body entanglement and dynamics at the energy scale of meV and light sources of highly-entangled, non-classical photons. We discovered that the optimal polariton interaction is realized near the crossover between photon blockade and polariton blockade for single-QD in each cavity.

The fluctuation effects may cause difficulties in realization of quantum phase transition from BEC to Mott insulator. On the other hand, it was shown that fluctuations in coupled cavity systems can lead to polaritonic glass phases [7]. The interplay between disorder and interaction effects in localization of bosonic particles is an interesting physics problem that has been studied for a long time but unsolved. This regime is also related to many-body localization which is an area gaining significant attention recently [48]. In the other limit, even a few coupled cavities [44] can provide a platform for quantum simulation of strongly interacting few-particle bosonic systems and serve as multi-photon entanglement light sources [49]. Finally, we remark that recent experiments have shown that exciton–exciton interaction can be tuned via the density of coexisting electrons (or holes) in QDs [50], offering additional tunability of the system.

## Acknowledgments

HXW and JHJ acknowledge support from the National Natural Science Foundation of China (grant no. 11675116) and the Soochow University. JHJ also thanks Sajeev John, Gang Chen, and Ming-Qi Weng for helpful discussions. AZ and AM are supported by the National Science Foundation under grant NSF-EFRI-1433496; and the Air Force Office of

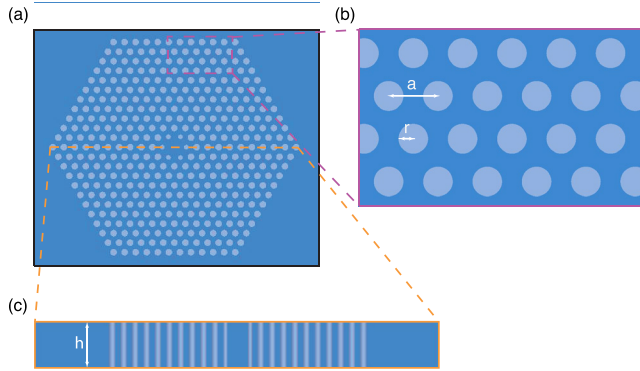


**Figure A1.** (a) Top-down view of the H1 cavity. The cavity is fabricated from a mother board of 2D triangle photonic crystal membrane. The lattice constant of the photonic crystal is  $a$  (b). The thickness of the film is  $h = 0.58a$ . (c). The radii of most of the air holes are  $r = 0.3a$ . The H1 cavity is formed by filling the central hole and reducing the radii of the nearest six air holes to  $r' = 0.21a$ . Those holes are shifted away from the center of the cavity by  $0.085a$ .

Scientific Research-Young Investigator Program under grant FA9550-15-1-0150. AM also acknowledges useful discussions with Xiaodong Xu. WLY acknowledges support by the Natural Science Foundation of Jiangsu Province of China under Grant No. BK20141190 and the National Science Foundation of China under Grant No. 11474211. YDX and HYC thank support from the National Science Foundation of China for Excellent Young Scientists (no. 61322504).

### Appendix A. Structure of the H1 cavity

The H1 cavity is designed in [25] which simultaneously has small modal volume, high Q-factor, and considerable coupling to detective optical apertures and fibers. The balance of those advantages enable strong light-matter interaction, photon/polariton blockade, and optical measurement facilities. The structure of the H1 cavity is illustrated in figure A1. The mother board is a 2D triangle lattice photonic crystal membrane with thickness  $h = 0.58a$  where  $a$  is the lattice constant. Most of the air holes have radii of  $r = 0.3a$ . The localized cavity mode is formed by filling the central air hole. To optimize the properties of the cavity mode the six air holes close to the center of the cavity have reduced radii  $r' = 0.21a$ . In addition, they are shifted away from the center of the cavity [25] by  $0.085a$ . The fundamental mode is a dipole-like mode of which most of the electromagnetic energy is in the electric field along the  $y$  direction [25]. This mode has frequency  $0.29\frac{2\pi c}{a}$  and Q-factor of 15000.

The energy scale of interaction and photon hopping must be much greater than the linewidths of cavity photon and QD exciton for quantum simulation to survive photon and exciton decay. The H1 cavity can have quality factor as high as  $2 \times 10^4$  [25], allowing energy resolution as low as 0.05 meV. The exciton decay in the cavity is dominated by exciton nonradiative relaxation. In monolayer MoS<sub>2</sub> the nonradiative decay lifetime is about 70 ps [51], providing a lower bound on the hopping and interaction energy of 0.01

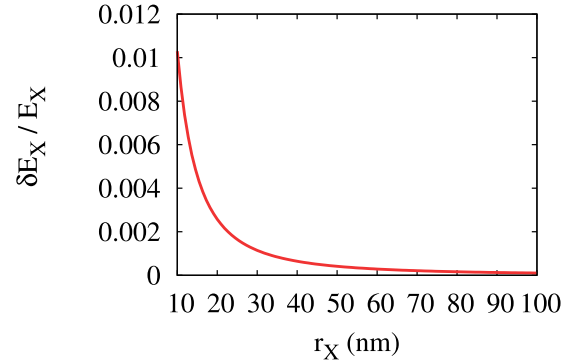


**Figure B1.** Modification of exciton energy  $\delta E_X/E_X$  as a function of QD radius  $r_X$  for MoS<sub>2</sub> QD.

meV. We consider the regime with hopping energy in the range  $0.5 \sim 1$  meV [52].

### Appendix B. Quantum confinement effect on exciton-polaritons

We have ignored the quantum nature of exciton (center-of-mass) wavefunction in estimations in the main text. If we consider a cylindrical QD, the ground state wavefunction is of the form,  $\psi(r) = \frac{1.087}{R} J_0(2.405 \frac{r}{r_X})$  [20] where  $J_0$  is the zeroth order Bessel function. The effective area of this wavefunction is  $S = \pi(0.69r_X)^2$ . The effective radius is then reduced to  $0.69r_X$ . Therefore, the optimal polariton repulsive interaction for MoS<sub>2</sub> in figure 1(b) can be realized for  $r_X \simeq 20$  nm which is achievable within the current fabrication technology [43].

The confinement also modifies the exciton energy  $E_X \equiv \hbar\omega_X$ . If excitons and photons are nearly in resonance, the photon energy  $\hbar\omega_c$  is also different. The exciton-photon interaction, which depends on  $\hbar\omega_c$ , is also modified. We need to examine how much modification of  $E_X$  is introduced by the confinement. The result is presented in figure B1, where we estimate the change of the exciton energy via,  $\delta E_X \sim \frac{\hbar^2 \pi^2}{2r_X^2 m_e} + \frac{\hbar^2 \pi^2}{2r_X^2 m_h}$ . The effective mass for electron and hole are  $m_e = 0.346m_0$  and  $m_h = 0.441m_0$ , respectively [60]. We plot  $\delta E_X/E_X$  as a function of  $r_X$  in figure B1. It is seen that the modification is within  $\sim 1\%$ , which means the confinement correction to exciton-photon coupling is negligible. However, the confinement may have significant effect on the fluctuation of the exciton energy if QD size fluctuates considerably. It was demonstrated in a recent experiment that precise control of QD size is achievable and the variation of QD size can be much reduced [43].

### Appendix C. Comparison with other strong light-matter interacting materials

The dipole matrix element  $d_{cv}$  of MoS<sub>2</sub> is deduced from the experimentally measured exciton-photon interaction in Fabry-Pérot cavity [53]. The Fabry-Pérot cavity is made of SiO<sub>2</sub>/Si<sub>3</sub>N<sub>4</sub> distributed Bragg reflector, in the middle there are two SiO<sub>2</sub> spacer layers above and below the MoS<sub>2</sub> monolayer.

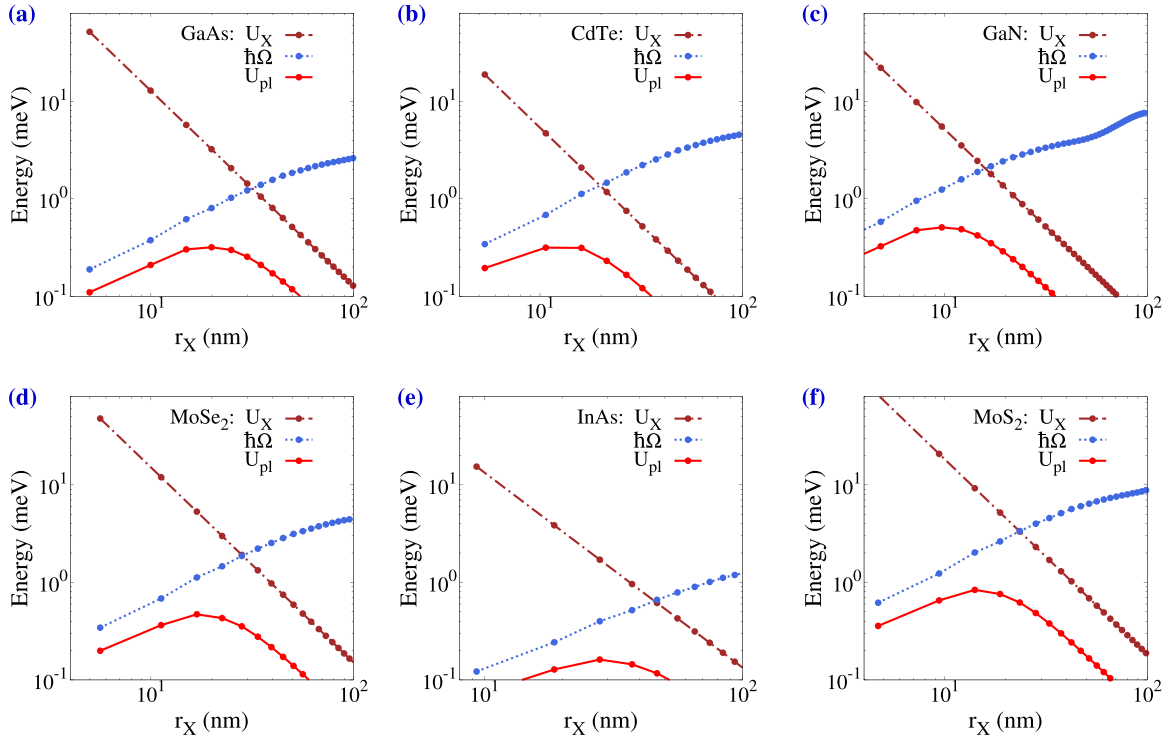


**Figure C1.** Exciton–exciton interaction  $U_X$ , exciton–photon interaction  $\hbar\Omega$ , and polariton–polariton interaction  $U_{pl}$  as functions of the QD radius  $r_X$  for GaAs (a), CdTe (b), GaN (c), MoSe<sub>2</sub> (d), InAs (e), and MoS<sub>2</sub> (f).

**Table C1.** Material parameters for GaAs, CdTe, InAs, MoSe<sub>2</sub>, GaN and MoS<sub>2</sub> in H1 cavity at zero exciton–photon detuning.

Material	$l$ (nm)	$d_{cv}$ (C · m)	$ \phi(0) $ (m <sup>-1</sup> )	$\hbar\omega_X$ (eV)	$a_B$ (nm)	$E_b$ (meV)
MoS <sub>2</sub>	0.65	$4.5 \times 10^{-29}$	$0.80 \times 10^9$	1.87	1.0	960.
MoSe <sub>2</sub>	0.7	$3.6 \times 10^{-29}$	$0.66 \times 10^9$	1.57	1.2	550.
GaAs	3.0	$12. \times 10^{-29}$	$0.098 \times 10^9$	1.76	8.4	9.5
CdTe	3.0	$10. \times 10^{-29}$	$0.23 \times 10^9$	1.65	3.5	22.9
InAs	3.0	$18. \times 10^{-29}$	$0.08 \times 10^9$	0.944	10.	7.0
GaN	1.3	$5.6 \times 10^{-29}$	$0.31 \times 10^9$	3.62	2.6	40.

We calculate the electric field intensity at the center of the cavity and determined the parameter  $d_{cv}$  by fitting the exciton–photon interaction to be 31.5 meV as measured in [53]. The Bohr radius of exciton in MoS<sub>2</sub> is  $a_B = 1$  nm as from [27]. The material parameters of GaAs and InAs are from the effective mass calculation using parameters in [54]. For CdTe the parameters are adopted from [14, 54]. The parameters for MoSe<sub>2</sub> is from [17, 26]. For GaN, the material parameters are derived from [55–57].

In figure C1 we plot the dependence of the exciton–photon interaction  $\hbar\Omega$ , exciton–exciton interaction  $U_X$ , and interaction between polaritons  $U_{pl}$  as functions of the QD radius  $r_X$  for GaAs, InAs, CdTe, MoSe<sub>2</sub>, and GaN when exciton and photon are in resonance. The optimal interaction between polaritons is estimated from those figures for various materials. The material parameters are adopted from experiments [55–58] and standard semiconductor handbooks [59]. The same H1 cavity is exploited for all materials (but with different lattice constant to ensure the resonance between exciton and cavity photon).

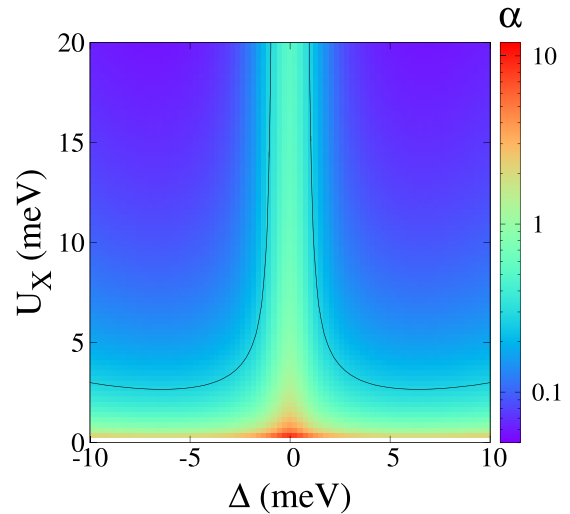


**Figure D1.** Quantum simulation in 1D Cavity-QD superlattices.  $\alpha$  and the phase diagram as functions of  $U_X$  and  $\Delta$ . Parameters:  $t = 1$  meV and  $\hbar\Omega = 10$  meV.

Material parameters of GaAs, CdTe, MoSe<sub>2</sub>, GaN and MoS<sub>2</sub> are listed in table C1. Here  $l$  is the thickness of the QDs along the  $z$  (growth) direction,  $d_{cv}$  is the interband dipole matrix element,  $|\phi(0)|$  is the exciton wave amplitude at zero electron-hole distance,  $\hbar\omega_X$  is the exciton energy,  $a_B$  is the exciton Bohr radius, and  $E_b$  is the exciton binding energy.

Since the exciton is set to be nearly in resonance with the fundamental mode of the H1 cavity, the ratio  $a/\lambda_X$  is a constant. The quantity  $g_X$  is a good measure of the exciton–photon interaction, and  $U_X^0$  is a good measure of the exciton–exciton interaction. From  $g_X$  we know that MoS<sub>2</sub> possesses the strongest exciton–photon interaction among the materials

listed in table 1. From the quantity  $U_X^0$  one can deduce that the exciton–exciton repulsion is the second strongest (only weaker than GaN). However, the wavelength for exciton emission in GaN is about half of that in MoS<sub>2</sub>. Therefore the geometry scale of the H1 cavity for GaN is half of that of MoS<sub>2</sub>, making fabrication of the H1 cavity for GaN more challenging. From this table one can already deduce that the optimal polariton interaction is largest in MoS<sub>2</sub>.

The advantages of MoS<sub>2</sub> monolayer QD also include the chemical and mechanical stability, the state-of-the-art fabrication technology that allows control of the position and of the lateral size of the QD [43], atomically-thickness, and spin-valley polarization [43].

#### Appendix D. Hamiltonian for superlattices of cavity–quantum-dot structures

The primary units of the superlattice is a pair of coupled cavities. We now compute polariton interaction  $U_{\text{pl}}$  in one such unit via equation (5). The ground state energy of two energy quanta in a pair of coupled cavities is obtained by diagonalizing the following Hamiltonian

$$H = 2\hbar\omega_X \hat{1} + \begin{pmatrix} 0 & \hbar\Omega & \hbar\Omega & 0 & -\sqrt{2}t & 0 & 0 & -\sqrt{2}t & 0 & 0 \\ \hbar\Omega & -\Delta & 0 & \hbar\Omega & 0 & -t & 0 & 0 & 0 & 0 \\ \hbar\Omega & 0 & \Delta & \hbar\Omega & 0 & 0 & 0 & 0 & -t & 0 \\ 0 & \hbar\Omega & \hbar\Omega & 0 & 0 & 0 & 0 & 0 & 0 & 0 \\ -\sqrt{2}t & 0 & 0 & 0 & 2\Delta & \sqrt{2}\hbar\Omega & 0 & 0 & 0 & 0 \\ 0 & -t & 0 & 0 & \sqrt{2}\hbar\Omega & \Delta & \sqrt{2}\hbar\Omega & 0 & 0 & 0 \\ 0 & 0 & 0 & 0 & 0 & \sqrt{2}\hbar\Omega & U_X & 0 & 0 & 0 \\ -\sqrt{2}t & 0 & 0 & 0 & 0 & 0 & 0 & -2\Delta & \sqrt{2}\hbar\Omega & 0 \\ 0 & 0 & -t & 0 & 0 & 0 & 0 & \sqrt{2}\hbar\Omega & -\Delta & \sqrt{2}\hbar\Omega \\ 0 & 0 & 0 & 0 & 0 & 0 & 0 & 0 & \sqrt{2}\hbar\Omega & U_X \end{pmatrix} \quad (\text{D.1})$$

where the ten basis states are  $|e(p); o(p)\rangle$ ,  $|e(p); o(X)\rangle$ ,  $|e(X); o(p)\rangle$ ,  $|e(X); o(X)\rangle$ ,  $|e(0); o(2p)\rangle$ ,  $|e(0); o(p+X)\rangle$ ,  $|e(0); o(2X)\rangle$ ,  $|e(2p); o(0)\rangle$ ,  $|e(p+X); o(0)\rangle$ , and  $|e(2X); o(0)\rangle$  where  $o$  and  $e$  denote the two cavities, respectively ( $p$  denotes photon, and  $X$  denotes exciton;  $2p$  stands for two photon,  $p+X$  stands for a photon and an exciton, whereas  $2X$  represents two excitons). We consider the case of which the detuning in the even cavity is  $\Delta$  whereas the detuning in the odd cavity is  $-\Delta$ . Diagonalization of the Hamiltonian yields the ground state energy. By comparing the ground state energy with and without the exciton–exciton interaction  $U_X$  we are able to compute the polariton interaction  $U_{\text{pl}}$  via

$$U_{\text{pl}} \equiv E_{\text{GS}} - E_{\text{GS}}^{(0)}, \quad (\text{D.2})$$

where  $E_{\text{GS}} (E_{\text{GS}}^{(0)})$  is the ground state energy for a single cavity with two quanta including (without) the exciton–exciton repulsion.

We determine the phase boundary for the BEC state and the Mott insulator state via the criterion  $t_{\text{pl}}/U_{\text{pl}} = \alpha_c$  for filling factor  $\nu = 1/2$ . The hopping amplitude  $t_{\text{pl}}$  is determined numerically by the energy difference for two pairs of cavities with and without hopping between them. The interaction energy  $U_{\text{pl}}$  is calculated via the above Hamiltonian (D.1) and the equation (5). The Mott insulator phase is realized in the regime with both strong exciton–exciton interaction  $U_X$  and large detuning  $|\Delta|$  (blue regions in figure D1). In other regimes polaritons are in the BEC phase. Particularly, for small detuning the system is always in the BEC phase even though the exciton repulsion  $U_X$  is large. Thus only for large detuning  $|\Delta|$  polaritons are confined in odd or even cavities and the Mott transition at the filling factor  $\nu = 1/2$ .

#### ORCID iDs

Jian-Hua Jiang  <https://orcid.org/0000-0001-6505-0998>

#### References

- [1] Feynman R P 1982 *Int. J. Theor. Phys.* **21** 467
- [2] Greiner M, Mandel O, Esslinger T, Hansch T W and Bloch I 2002 *Nature* **415** 39
- [3] Bloch I, Dalibard J and Nascimbene S 2012 *Nat. Phys.* **8** 267
- [4] Chang D E, Vuletić V and Lukin M D 2014 *Nat. Photon.* **8** 685
- [5] Hartmann M J, Brandao F G S L and Plenio M B 2006 *Nat. Phys.* **2** 849
- [6] Angelakis D G, Santos M F and Bose S 2007 *Phys. Rev. A* **76** 031805
- [7] Rossini D and Fazio R 2007 *Phys. Rev. Lett.* **99** 186401
- [8] Noh C and Angelakis D G 2016 *Rep. Prog. Phys.* **80** 016401
- [9] Carusotto I and Ciuti C 2013 *Rev. Mod. Phys.* **85** 299
- [10] Buckley S, Rivoire K and Vučković J 2012 *Rep. Prog. Phys.* **75** 126503

- [11] Byrnes T, Kim N Y and Yamamoto Y 2014 *Nat. Phys.* **10** 803
- [12] Rundquist A et al 2014 *Phys. Rev. A* **90** 023846
- [13] Wen X G 2004 *Quantum Field Theory of Many-Body Systems* (Oxford: Oxford University Press)
- [14] Jiang J-H and John S 2014 *Phys. Rev. X* **4** 031025
- [15] Kasprzak J et al 2006 *Nature* **443** 409
- [16] Balili R, Hartwell V, Snoke D, Pfeiffer L and West K 2007 *Science* **316** 1007
- [17] Jiang J H and John S 2014 *Sci. Rep.* **4** 7432
- [18] Nguyen H S et al 2013 *Phys. Rev. Lett.* **110** 236601
- [19] Ballarini D et al 2013 *Nat. Commun.* **4** 1778
- [20] Verger A, Ciuti C and Carusotto I 2006 *Phys. Rev. B* **73** 193306
- [21] Birnbaum K M, Boca A, Miller R, Boozer A D, Northup T E and Kimble H J 2005 *Nature* **436** 87
- [22] Faraon A, Fushman I, Englund D, Stoltz N, Petroff P and Vučković J 2008 *Nat. Phys.* **4** 859
- [23] Reinhard A, Volz T, Winger M, Badolato A, Hennessy K J, Hu E L and Imamoglu A 2012 *Nat. Photon.* **6** 93
- [24] Müller K et al 2015 *Phys. Rev. Lett.* **114** 233601
- [25] Hagemeyer J et al 2012 *Opt. Exp.* **20** 24714
- [26] Dufferwiel S et al 2015 *Nat. Commun.* **6** 8579
- [27] Qiu D Y, da Jornada F H and Louie S G 2013 *Phys. Rev. Lett.* **111** 216805
- [28] Tassone F and Yamamoto Y 1999 *Phys. Rev. B* **59** 10830
- [29] Kühner T D and Monien H 1998 *Phys. Rev. B* **58** R14741
- [30] Majumdar A et al 2011 *Phys. Rev. B* **84** 085309
- [31] Gardiner C and Zoller P 2004 *Quantum Noise* 3rd edn (Berlin: Springer)
- [32] Tomadin A, Giovannetti V, Fazio R, Gerace D, Carusotto I, Türeci H E and Imamoglu A 2010 *Phys. Rev. A* **81** 061801
- [33] Carusotto I, Gerace D, Türeci H E, De Liberato S, Ciuti C and Imamoglu A 2009 *Phys. Rev. Lett.* **103** 033601
- [34] Hartmann M J 2010 *Phys. Rev. Lett.* **104** 113601
- [35] Grujic T, Clark S R, Angelakis D G and Jaksch D 2012 *New J. Phys.* **14** 103025
- [36] Boité A L, Orso G and Ciuti C 2013 *Phys. Rev. Lett.* **110** 233601
- [37] Hartmann M J, Brandao F G S L and Plenio M B 2008 *Laser Photon. Rev.* **2** 527–56
- [38] Hartmann M J 2016 *J. Opt.* **18** 104005
- [39] Weisbuch T C, Dingle R, Gossard A C and Wiegmann W 1981 *Solid State Commun.* **38** 709–12
- [40] Mak K F, Lee C, Hone J, Shan J and Heinz T F 2010 *Phys. Rev. Lett.* **105** 136805
- [41] Wang Q H, Kalantar-Zadeh K, Kis A, Coleman J N and Strano M S 2012 *Nat. Nanotechnol.* **7** 699
- [42] Xu X, Yao W, Xiao D and Heinz T F 2014 *Nat. Phys.* **10** 343
- [43] Wei G et al 2017 *Sci. Rep.* **7** 3324
- [44] Wu S et al 2015 *Nature* **520** 69
- [45] Dumcenco D et al 2015 *ACS Nano* **9** 4611
- [46] Noda S, Fujita M and Asano T 2007 *Nat. Photon.* **1** 449
- [47] Amani M et al 2015 *Science* **350** 1065
- [48] Oganessian V and Huse D A 2007 *Phys. Rev. B* **75** 155111
- Pal A and Huse D A 2010 *Phys. Rev. B* **82** 174411
- Altman E and Vosk R 2015 *Ann. Rev. Condens. Matter Phys.* **6** 383
- [49] Pan J-W, Chen Z-B, Lu C-Y, Weinfurter H, Zeilinger A and Zukowski M 2012 *Rev. Mod. Phys.* **84** 777
- [50] Sidler M et al 2017 *Nat. Phys.* **13** 255
- [51] Shi H et al 2013 *ACS Nano* **7** 1072
- [52] Majumdar A, Rundquist A, Bajcsy M, Dasika V D, Bank S R and Vučković J 2012 *Phys. Rev. B* **86** 195312
- [53] Liu X, Galfsky T, Sun Z, Xia F, Lin E-c, Lee Y-H, Kéna-Cohen S and Menon V M 2015 *Nat. Photon.* **9** 30
- [54] Vurgaftman I, Meyer J R and Ram-Mohan L R 2001 *J. Appl. Phys.* **89** 5815
- [55] Feltin E, Christmann G, Butté R, Carlin J-F, Mosca M and Grandjean N 2006 *Appl. Phys. Lett.* **89** 071107
- [56] Bigenwald P, Lefebvre P, Bretagnon T and Gil B 1999 *Phys. Status Solidi b* **216** 371
- [57] Chung T-Y and Chang K J 1998 *Semicond. Sci. Technol.* **13** 876
- [58] Ugeda M M et al 2014 *Nat. Mater.* **13** 1091
- [59] Madelung O (ed) 1987 *Semiconductors (Landolt-Börnstein, New Series)* (Berlin: Springer)
- [60] Cheiwchanchamnangij T and Lambrecht W R 2012 *Phys. Rev. B* **85** 205302